Femtosecond conformational changes in a photolyase guide long-range electron transfer as resolved by serial crystallography

Andrea Cellini
University of Gothenburg
Madan Kumar Shankar
Uppsala University
Amke Nimmrich
University of Gothenburg
Jennifer Mutisya
Uppsala University
Antonia Furrer
Paul Scherrer Institut,
Emma Beale
Paul Scherrer Institut,
Melissa Carrillo
Paul Scherrer Institut, https://orcid.org/0000-0002-0744-4486
Tek Narsingh Malla
University of Wisconsin Milwaukee https://orcid.org/0000-0002-1387-0801
Piotr Maj
Department of Chemistry-BMC https://orcid.org/0000-0002-9832-2344
Lidija Vrhovac
Department of Chemistry-BMC
Florian Dworkowskic
Paul Scherrer Institut
Claudio Cirelli
Paul Scherrer Institute https://orcid.org/0000-0003-4576-3805
Philip Johnson
Paul Scherrer Institut https://orcid.org/0000-0002-7251-4815
Dmitry Ozerov
Paul Scherrer Institut https://orcid.org/0000-0002-3274-1124
Camila Bacellar
Paul Scherrer Institute https://orcid.org/0000-0003-2166-241X
Jörg Standfuss

Paul Scherrer Insitute https://orcid.org/0000-0001-8825-386X
Marius Schmidt
Univ of Wisconsin, Milwaukee https://orcid.org/0000-0002-0962-9468
Tobias Weinert
Paul Scherrer Institut
Janne Ihalainen
University of Jyväskylä https://orcid.org/0000-0002-8741-1587
Weixiao Wahlgren
University of Gothenburg
Sebastian Westenhoff (sebastian.westenhoff@kemi.uu.se)
University of Gothenburg https://orcid.org/0000-0002-6961-8015

Article

Keywords:

Posted Date: February 14th, 2023

DOI: https://doi.org/10.21203/rs.3.rs-2491087/v1

Additional Declarations: There is **NO** Competing Interest.

Version of Record: A version of this preprint was published at Nature Chemistry on January 15th, 2024.
See the published version at https://doi.org/10.1038/s41557-023-01413-9.

Femtosecond conformational changes in a photolyase guide long-range electron transfer as resolved by serial crystallography

Andrea Cellini[1], Madan Kumar Shankar[1,2], Amke Nimmrich[1], Jennifer Mutisya[1,2], Antonia Furrer[3], Emma V. Beale[3], Melissa Carrillo[3], Tek Narsingh Malla[4], Piotr Maj[1,2], Lidija Vrhovac[1,2], Florian Dworkowskic[3], Claudio Cirelli[3], Philip Johnson[3], Dmitry Ozerov[3], Camilla Bacellar[3], Jörg Standfuss[3], Marius Schmidt [4], Tobias Weinert[3], Janne A. Ihalainen[5], Weixiao Yuan Wahlgren[1] & Sebastian Westenhoff[1,2,*].

[1] Department of Chemistry and Molecular Biology, University of Gothenburg Box 462, 40530 Gothenburg, Sweden.

[2]Department of Chemistry-BMC, University of Uppsala, Husargatan 3, 752 37 Uppsala.

[3]Paul Scherrer Institut, 5232 Villigen, Switzerland.

[4]Physics Department, University of Wisconsin-Milwaukee, 3135 N. Maryland Ave, Milwaukee, Wisconsin 53211, USA.

[5]Department of Biological and Environmental Sciences, Nanoscience Center, University of Jyvaskyla, Box 35, 40014 Jyvaskyla, Finland.

[*]corresponding author. E-mail:sebastian.westenhoff@kemi.uu.se

Abstract

Charge transfer reactions in proteins are fundamentally important for life, but it is currently not clear how protein structural dynamics control these electron transfer reactions. Photolyases/cryptochromes, which repair DNA and signal in all kingdoms of life, have a paradigm electron transfer cascade. Here, photoreduction of the flavin cofactor initiates charge transfer along a chain of four conserved tryptophans. We report femtosecond X-ray crystallographic snapshots for the *Drosophila melanogaster* (6-4) photolyase, revealing protein structural changes while electron transfer occurs. At femto- and picosecond delays, photoreduction of the flavin by the first tryptophan causes directed structural responses at key residue asparagine 403, at a conserved salt bridge, and by rearrangements of nearby water molecules. Along the tryptophan cascade, we detect charge-induced protein structural changes close to the second tryptophan from 1 ps to 20 ps, thereby identifying methionine 408 as an active participant in the redox chain, and from 300 ps around the fourth tryptophan. The data reveal that the protein undergoes highly directed and carefully timed adaptations of its structure to facilitate electron transfer. This suggests that evolution has optimized fast protein fluctuations for optimal function.

1 Introduction

Electron transfer (ET) in proteins is important in many biological processes, such as photosynthesis, cellular respiration, oxidative stress defense mechanism, and denitrification [1–3]. Electron transfer typically occurs in between co-factors or amino acid side chains and has been studied for decades [4, 5]. A paradigm for electron transfer reactions in proteins occurs in photolyases/cryptochromes, where a flavin adenine dinucleotide (FAD) cofactor is photoreduced and electrons are donated through a chain of conserved tryptophane residues [6–8].

Photolyases repair DNA lesions using light as energy source [9]. They are essential for maintaining the integrity of the genome in prokaryotes and many eukaryotes. Photolyases form a protein family together with cryptochromes, which regulate growth and development in plants, entrain the circadian clock to day light, and provide a key component to magnetovision in some animals [10, 11]. Despite their diverse functions, photolyases and cryptochromes have remained structurally homologous over billions of years of evolution. This testifies to the functional importance of the electron transfer chain to the protein family.

In both photolyases and cryptochromes, the photoexcited FAD extracts an electron from the nearby tryptophan 407 (count for the *Drosophila melanogaster* (6-4) photolyase) within one picosecond, initiating the cascade of ET reactions along Trp384, Trp330, and Trp381. A long-range (15 Å - 18 Å) radical pair between the semiquinone $FAD^{\cdot -}$ and the tryptophanyl radical $Trp381H^{\cdot +}$ is established within a few microseconds [8, 12]. In cryptochromes, this is the active signaling state, but in photolyases the photoreduction is repeated a second time, yielding $FADH^-$, which is the state that can repair the DNA lesion [13, 14]. For stabilization of the semiqunionone radical pair, the last tryptophan of the chain typically releases a proton to the surrounding solvent and gets deprotonated, and the $FAD^{\cdot -}$ receives a proton to form $FADH^{\cdot}$. Both processes occur on millisecond time scales [12, 15]. Electron transfer rates between the tryptophans have been determined [8, 12, 15] and more complex reaction pathways have been found, including side reactions to other tryptophans and the adenine group of the FAD [16].

According to Marcus theory, electron transfer reactions are controlled by the free energy gain and the ability of the transfer site and environment to stabilize the charge [17]. When electron transfer occurs on the same time scale as the environmental relaxation, the dynamics of these relaxations dictate the transfer kinetics [18]. Quantum mechanical theories of electron transfer largely confirm this notion [19]. In photolyases/cryptochromes the separation of the radical pair must be driven by structural dynamics of the transfer site or the protein, as the ionization potential of the transfer sites itself does not provide an energy funnel for charge transfer [20, 21]. Various models of electron transfer in photolyases have been proposed including those considering dynamic relaxation of the environment and tunneling of electrons [20, 22, 23]. However, understanding of the electron transfer in photolyases/cryptochromes beyond isotropic dielectric response theory is hindered by a lack of experimental data on dynamic structural changes.

The closest information on the subject comes from intraprotein solvation kinetics derived from time-dependent Stoke shift measurements [24, 25]. From these experiments it was concluded that waters respond to charge density changes within few picoseconds, that combined water and protein movements take tens of picoseconds, and that large scale breathing motions of the protein lead to solvation dynamics at hundreds of picoseconds. These data are, however, not structure specific and therefore a gap in understanding persists on how protein structural changes guide electron transfer reactions.

Femtosecond time-resolved serial crystallography opens up for studying the structural changes in the entire protein upon electron transfer [26, 27]. The technique has been used for deciphering structural mechanisms in photosynthetic, sensor, and transport proteins [28–33]. With respect to photolyases, a nanosecond time-resolved SFX study has been carried for the two reduction steps on a cis-syn cyclobutane pyrimidine dimer (CBD) photolyase [34], and we have recorded a crystallographic snapshot of the end state of the first photoreduction in a (6-4) photolyase at 100 ms [35]. Here, we capture structural snapshots for the (6-4) photolyase from *Drosophila Melanogaster* covering the earliest, femto- and picosecond time scales. We identify distinct protein structural changes, which accompany the electron transfer at the FAD and along the tetrad of tryptophans, visualizing how highly directed movements of amino acids and water molecules accompany electron transfer reactions in photolyases.

2 Results

Reliable DED signals are observed and propagate along the conserved tetrade.

First, we were curious to find out if the structural changes associated with electron transfer in photolyases can be determined by time-resolved SFX. We recorded time-dependent crystallographic data from microcrystals of *Dm*(6-4)photolyase, dispersed in a cellulose matrix. Photoexcitation was performed by an optical laser pulse with a pulse length of 150 fs, a center wavelength of 473 nm, and at a fluence of $1.4\,mJ/mm^2$. We observed difference electron density (DED) features above noise for all time points from femto- to microseconds (Fig. 1). Lowering the effective photon fluence by a factor of 1.8 reduced the signal and lowering it by a factor of 8 made it vanish (see Extended Fig. 1). We therefore conclude that the excitation fluence is in the regime of one-photon absorption.

In order to characterize how the DED evolves with time, we integrated the DED in each map for three regions of residues (Fig. 1C), which are defined in Fig. 1B. We found that the kinetics for the three regions are distinct: Region 1 is close to the chromophore (average distance of Cα from N5 of FAD was 4.5 Å) and has a maximum at the earliest time point of 400 fs, region 2 is close to the second tryptophan Trp384 (12.4 Å distance form N5) and tops at 20 ps, whereas region 3 around the last tryptophan 381 (20.0 Å from N5) rises at late time points (300 ps, and 100 μ). The observed DED changes are rather small and indicate time-dependent, concerted structural changes of a few residues around the key charge transfer sits. We conclude that the DED present proteins structural changes,

which follow the expected flow of electrons through the protein.

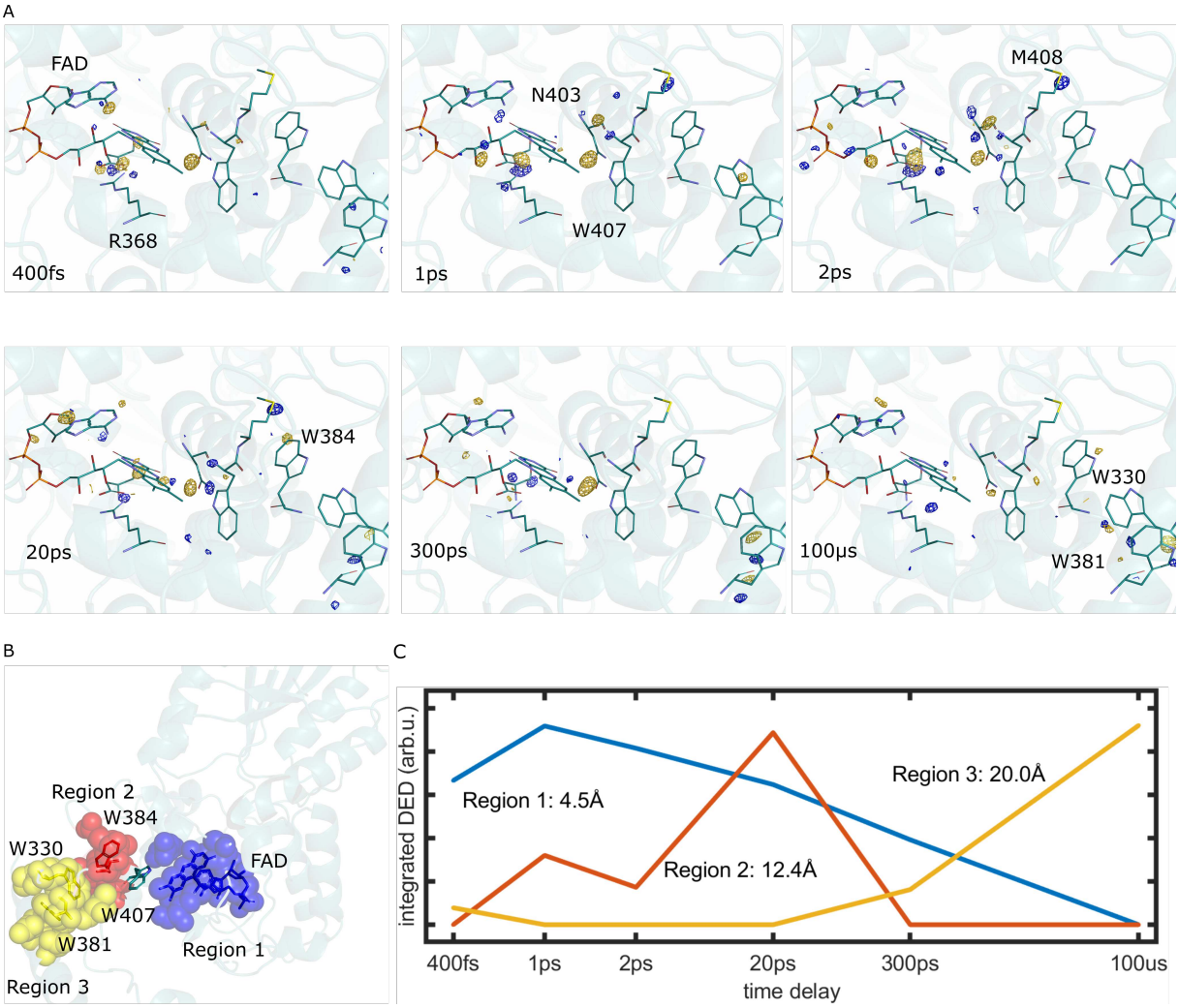

Figure 1: **Structural changes along the tetrade of tryptophans.** A: Observed DED obtained at 400 fs, 1 ps, 2 ps, 20 ps, 300 ps and 100 μs after light activation. The maps are contoured at 4σ. The dark structure is shown in cartoon representation with FAD and key residues in sticks. Negative and positive features are depicted in gold and blue, respectively. B: The residues for the three regions are indicated as spheres of different color. C: The integrated DED is displayed for the three regions. Integration was in a radius of 1 Å around the atoms of each region and for DED above 2.9 sigma of the map. Region 1: FAD, 368, 397, 403; Region 2: 384, 385, 408, 411, 413; Region 3: 328, 329, 330, 376, 381, 490.

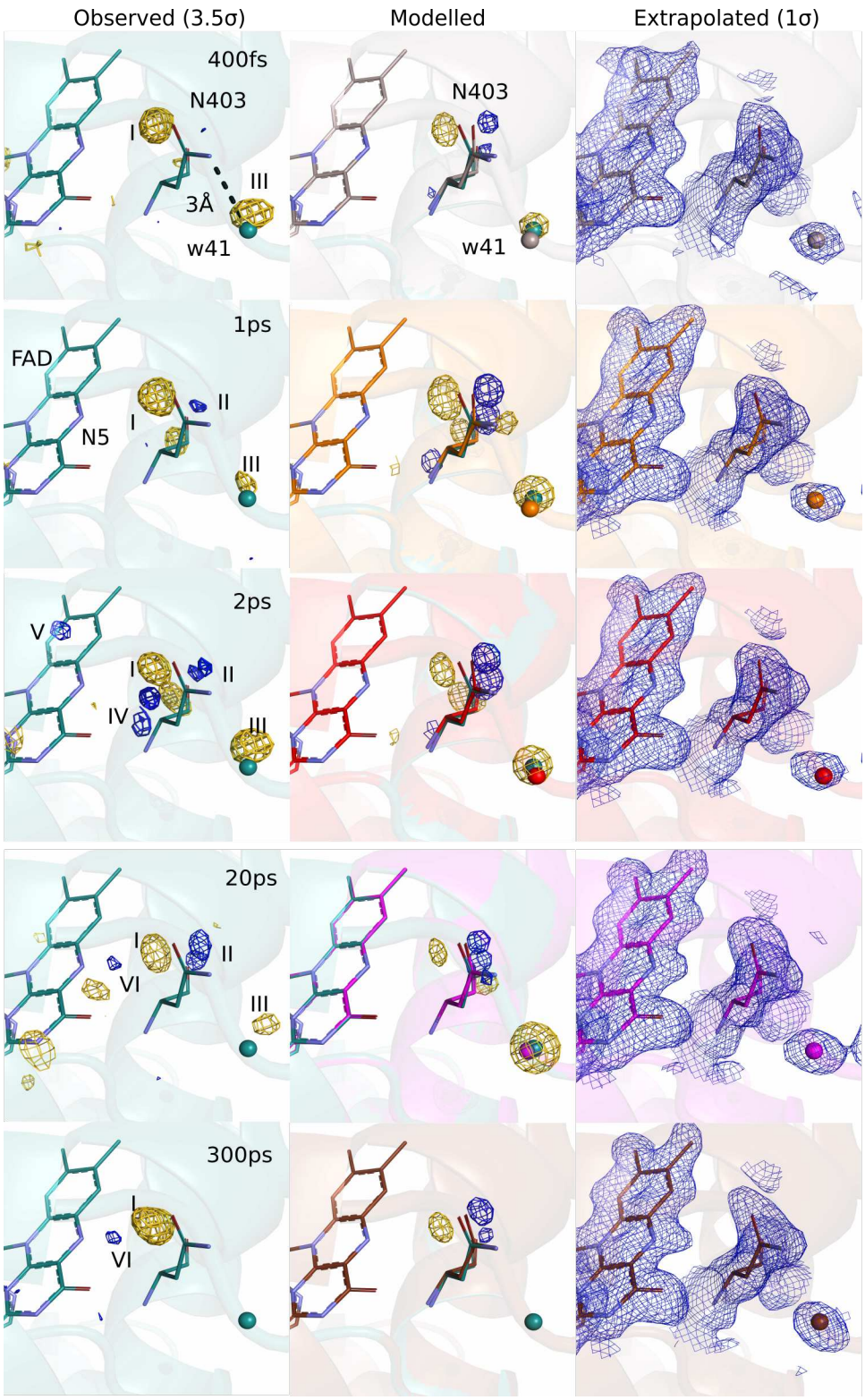

Figure 2: **Conformational changes around Asn403.** The dark structure (cyan) and the observed difference electron density maps are shown in the left column. The light structures superimposed with the dark structure and the calculated difference electron density maps are shown in the middle column. The negative and the positive features are depicted in gold and blue, respectively. The light structures and the 2Fe-Fc electron density maps (blue) of FAD, asparagine 403 (N403) and surrounding water molecule w41 are shown in the right column.

Table 1: Time-dependent distances (in Å) between various residues

Delay time	Asn403(C=O)-FAD(N5)	Asn403(NH_2)-FAD(N5)	Asn403-Trp407	Asp397(OD1)-Arg368(NH1)	Asp397(OD2)-Arg368(NH2)
dark	3.66	5.24	2.93	2.98	2.75
400 fs	4.17	5.24	2.93	3.15	2.89
1 ps	3.99	5.37	2.89	3.31	2.88
2 ps	4.12	5.23	2.80	3.27	2.80
20 ps	3.87	5.21	2.88	3.10	2.68
300 ps	3.92	5.30	2.86	3.06	2.46

Structural stabilization of the photoinduced charge on the FAD. Next, we focus on the DED features observed close the FAD chromophore. Spectroscopic data indicate that photoactivation leads to electron transfer from Trp407 to FAD within less than 0.8 ps [12, 36, 37]. Close to N5 of the FAD and the first tryptophan (Trp407) of the tetrad, we observe strong DED features on asparagine 403 (Asn403) at 400fs, 1 ps, 2 ps, 20 ps and 300 ps (Fig. 2, feature I and II) (Fig. 1). Residues at the position of Asn403 are known to be crucial for stabilization of the charge on the FAD in photolyases/cryptochromes. To visualize the time-dependence of the DED features, we integrated the DED in a radius of 2 Å around Asn403 (Fig. 4C) [38]. The kinetics of Asn403 show an instantaneous signal, a further rise up to 20 ps, and a decay for later time points. We refined Asn403 using real-space refinement against extrapolated maps (third column in Fig. 2), using visual agreement between experimental (first column in Fig. 2) and calculated DED maps (second column in Fig. 2) to ensure good fits. From 400 fs to 20 ps the side chain of Asn403 twists, so that the carbonyl group moves away and the amino group moves closer to FAD-N5 (Table 1). Water 41, which is in hydrogen bonding distance to the amino group of Asn403 and faces away from the FAD in the dark structure, follows this movement (Fig. 2, feature III). We attempted several other movements of Asn403 including a different rotamer, or moving the carbonyl group much closer to the N5 of the FAD into H-bond distance, but the alternative models did not lead to good agreement between the observed and calculated DED (Fig. Extended Fig. 2). We conclude that the side chain of Asn403 reacts to the change in electrostatics when the FAD becomes reduced. However, it does not undergo a change big enough to stabilize the FAD^- through a direct hydrogen bond.

Water dynamics around FAD. In addition to the movement of Asn403 itself, we observe several positive DED features between the Asn403 and the N5 of the FAD. These are most pronounced (>3.5 sigma) at 20 ps and 300 ps (Fig 2, feature VI) and also present at 2 ps albeit in different shape and positions (feature IV and V). We attribute these DED features to water molecules which occupy the space between Asn403 and the N5, thereby H-bonding to the negatively charged N5 and stabilizing the charge on the $FAD^{\cdot-}$ on picosecond time scales.

The kinetics of these positive DED features are interesting (Fig 4B). At time delays 400 fs and 1 ps no discernible positive DED features are observed, feature IV and V are only present transiently at 2 ps, and feature IV arises after this time point. The water response in the chromophore binding pocket is delayed with respect to the response of the side chain of Asn403 and the charge transfer time. It is dynamic in time and space, indicating that the water traverse through a series of states to reach their final positions.

Ultrafast response of the Asp397:Arg368 salt bridge. Next, we turn our attention to the conserved salt bridge between Asp397 and Arg368, which is located on the opposing side of the FAD compared to Asn403. Fig. 3A illustrates a movement of the side chain Asp397 through the correlated positive and negative features VII, which are present at 400 fs, maximal at 1 ps and 2 ps, muted at 20 ps, and which has decayed below noise by 300 ps (Fig. 4B). Refined light structures indicate a transient distance increase across the salt bridge caused by rotation of Asp397 (Table 1). We did not detect a light induced interaction between Arg368 and the FAD, which was observed on microsecond time scales [34]. Since the response of the salt bridge is present at 400 fs and quickly decays, we conclude that it is an effect of the sudden change of electrostatics on the reduced FAD.

Picosecond conformational changes of the FAD chromophore. On the FAD itself, we do not detect strong signals that can be attributed to the bending of the isoalloxazine ring of the FAD. We observe some negative features on the pyrophosphate chain at 1 ps and 2 ps, but the meaning of those signals is not clear. At 2 ps, 20 ps and 300 ps we find correlated positive and negative DED close to a cluster of water molecules (w70) (Fig. 3C). We attribute this to be a signature of transient oxidation of the adenine through electron transfer to the isoalloxazine ring of the FAD, as has been observed spectroscopically on picosecond time scales [12]. The refined positions of the water molecules show that the a hydrogen bond between the adenine and water 70, which is present in dark, is broken in this process (Fig. 3C).

Protein response along the tryptophan tetrade. We now turn our attention to changes along the tryptophan tetrad. As in the previous serial crystallographic experiments on photolyases [34, 35], we did not observe DED signals on the tryptophan side chains itself above 3.5σ, except for signals on the fourth tryptophan (Trp381) from 20 ps (Fig. 1 and Extended Fig. 4). In particular and related to the first electron transfer step from Trp407 to the FAD, which occurs in less than 0.8 fs, we did not observe changes in the reciprocal distance between either the FAD and Trp407 or between Asn403 and Trp407 (Table 1). This indicates that the protein environment of Trp407 is either very rigid, or that the second tryptophan donates its electron extremely quickly to Trp407.

From 1 ps up to 20 ps, we observe a strong positive signal next to the sulfur atom of the conserved methionine (M408, Fig. 3B). The feature has a delayed rise (maximum at 2 ps), and decays to zero amplitude until 300 ps (Fig. 4B). The sulfur atom of Met408 is located only 4.1 Å from the Trp384 side chain. The signal consists of a positive DED (Fig. 3B), which can be explained by the dynamic localization of an atom in the positive density. We propose that the change is due to a water molecule, which localizes closely to the methionine sulfur atom of Met408 and transiently oxidizes it.

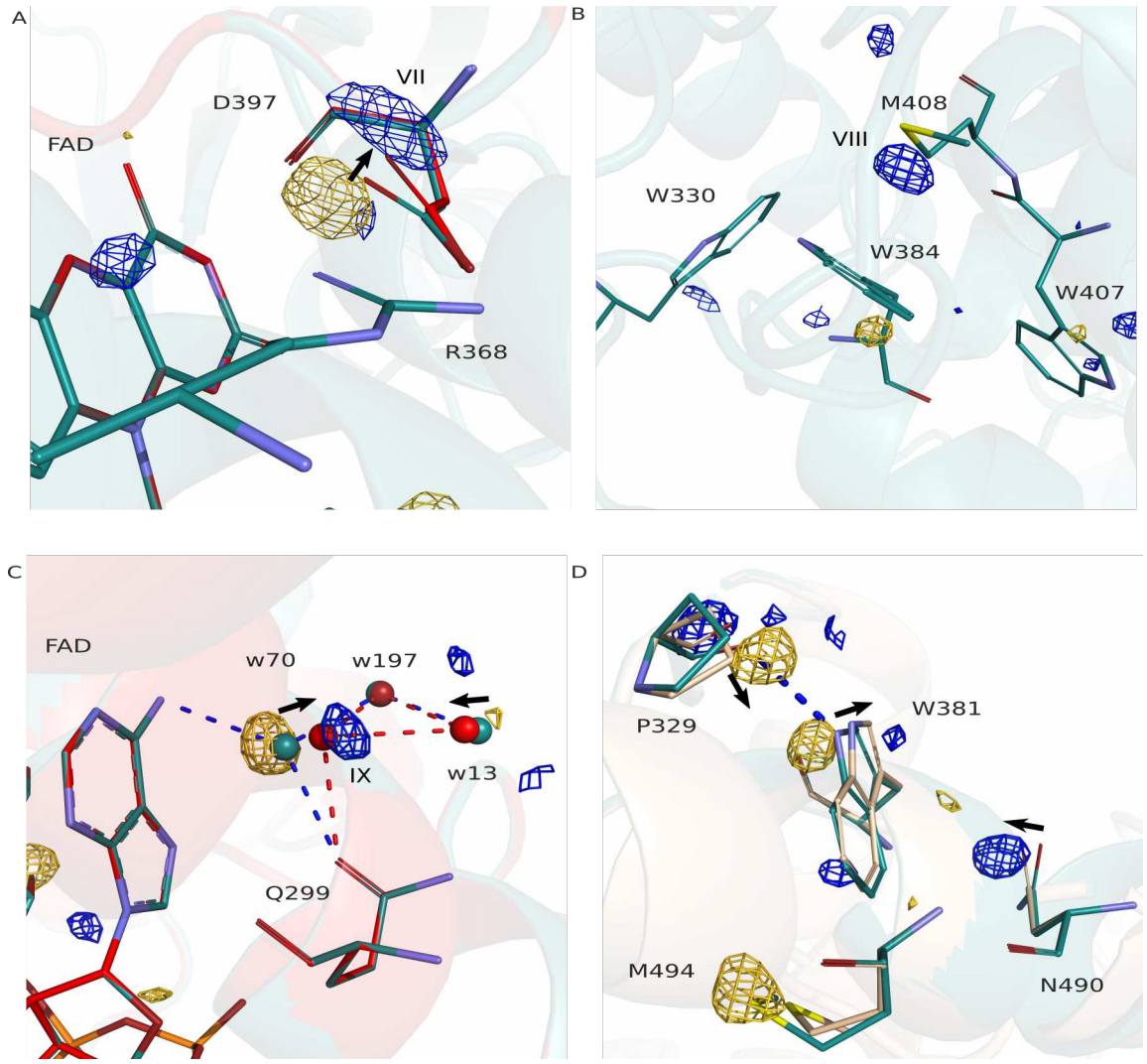

Figure 3: **Femto- to microsecond conformational changes around key residues.** A. Observed DED at 2 ps and 3.5σ with the dark structure (cyan) superimposed on the light structure (red) obtained at 2 ps. B. Observed DED map around Met408 at 20 ps is displayed together with the dark structure (cyan), contoured at 3.5σ. C. Observed DED at 2 ps and 3.5σ around the adenine moiety of the FAD, with the dark structure (cyan) superimposed on the light structure (red). Hydrogen-bonding networks of the FAD, Gln299 and water molecules w70, w197 and w13 are shown in blue dashed line in the dark structure and red in the light structure. D. Observed DED map and superimposed dark (cyan) and light (yellow) models around the final tryptophan Trp381 at 100μs. Hydrogen bond between the backbone of Pro329 and Trp381 in the dark structure is shown in dashed line (blue). In all maps, the negative and the positive features are depicted in gold and blue, respectively. Arrows indicate movement of atoms upon photoexcitation.

Finally, the data reveals prominent DED features at the fourth tryptophan (Trp381) in the late time point (100μs) (Fig. 3D and S5), with a small signal present already at 20 ps, and 300 ps (Fig 1 and (Fig. 4B). At 100 μs, we detect structural changes at Trp381, Pro329, Asn490 and Met494, indicating

that the hydrogen bond between Pro329 and Trp381 in the dark state breaks [35], that the side chain of Trp381 moves, and that Asn490 is moving closer to Trp381. We interpret these changes to be due to the arrival of the charge to the last tryptophan Trp381. The DED around Trp381 is weaker than what we detected previously at 100 ms, but features appear at similar positions (Fig. S5) [35]. Based on this and consistent with the expected electron arrival time [12], we assign Trp381 to be in its cationic radical state ($TrpH^{\cdot+}$), before deprotonation to the solvent occurs. The signal on the final trpytophan at 100 μs also serves as an internal reference for the present measurements: existence of the signal implies that the photoexcitation yielded in the crystal is notable and that the DED follows the expected flow of electrons through the protein.

3 Discussion

Photolyases harvest solar energy in a two-step photoreduction process to then be able to repair DNA lesions. The protein thereby balances two partially opposing objectives. Charge recombination has to be minimized for maximal collection efficiency, which is achieved by swift separation of charges into the long-range radical pair. At the same time, the charges have to remain accessible for repairing DNA lesions. This implies that the radicals should not be trapped in deep energy minima, which would render the subsequent processes less effective. These are the same requirements as in photosynthetic proteins, where photogenerated charges have to be transported to opposite sites of the membrane.

In photolyases and cryptochromes, the electrons transfer between similar tryptophan side chains and thus the free energy gain per transfer step is low at a maximum of 10 kcal/mol, depending on the transfer step [12, 39]. The reorganziation energy is on the order of 20-30 kcal/mol for the forward reactions [12, 39]. This indicates that the charge transfer is driven by the dynamic solvation of the transfer site and its environment, of which we resolve atomic motions in the protein.

Here, we discover a series of timed and specific responses upon charge transfer, which we summarize in Fig. 4. The highly conserved salt bridge Asp397:Arg368 shows the fastest response to photoreduction of the FAD (event 1). It is present from 400 fs onwards and decays until 300 ps. The second fastest response is for Asn403 (event 2). Asn403 is conserved among CPD and (6-4) photolyases, and substituted into an aspartate in plant cryptochrome, and a cysteine in *Dm* cryptochrome. The residue was found to form a H-bond to FAD in its semiquinone state [34, 35]. Here, we establish that Asn403 does not reach direct hydrogen bonding interaction with the N5 of the FAD on picosecond time scales, contrary to what could have been envisaged [40]. Thirdly, water molecules localize close to the N5, likely to H-bond to it (event 3). The time scale of the water solvation is consistent with expectations [41]. While the decay of water feature IV follows the decay kinetics of Asn403 and $FAD^{\cdot-}$, the build-up of the water scaffold is more delayed and more complex, involving different sites around the N5. Hereby, water position 1 (feat V) is populated first at 2 ps and wat 2 (feat IV) takes over afterwards (Fig. 4B).

These three events, which stabilize the charge on FAD^{-}, are not only coordinated in space, but also

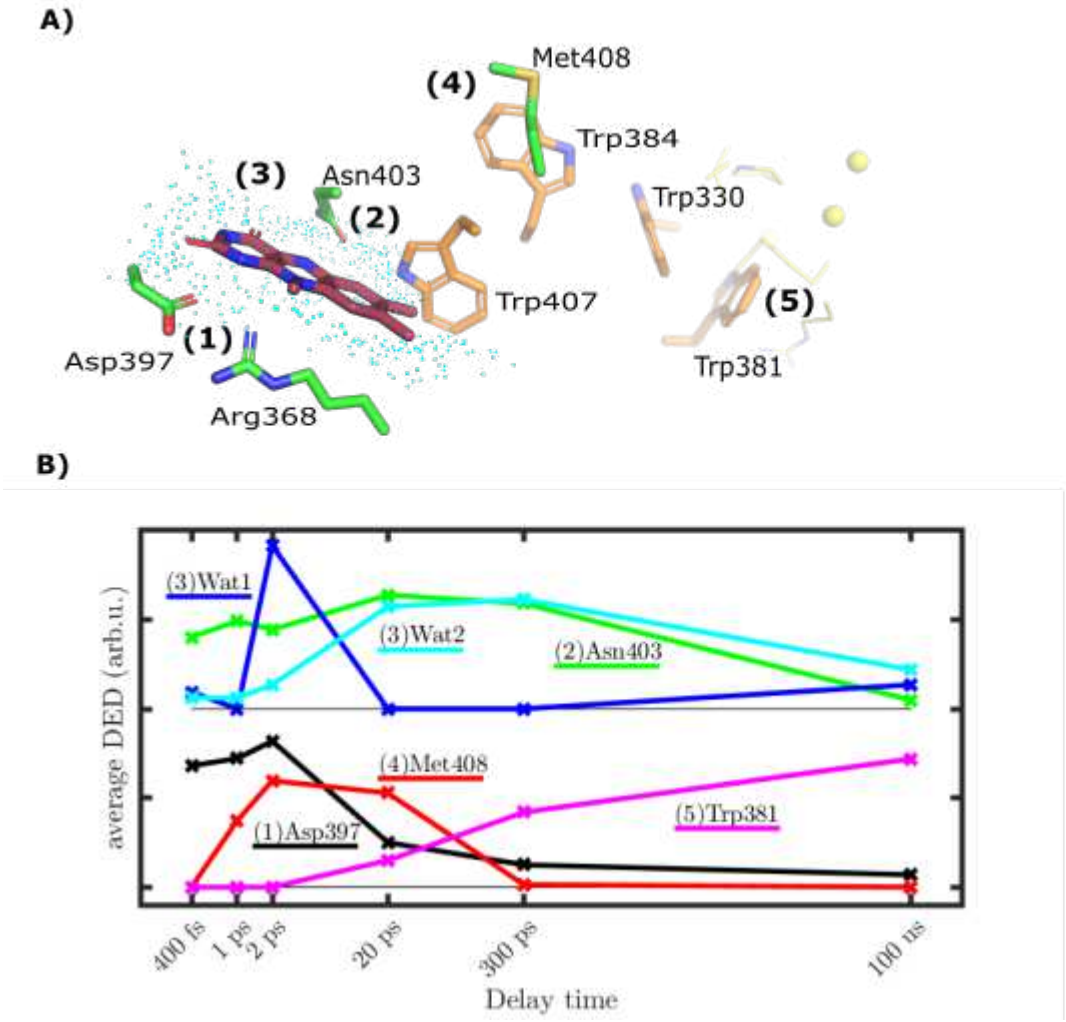

Figure 4: **Summary of photochemical events.** A. Denotes key residues and processes. (1) FAD is reduced and Asp397 and Arg368 respond immediately. (2) Asn403 reacts similarly fast and undergoes a slow phase of response up to 20 ps, (3) a delayed (from 1 ps) and complex motion of water molecules is completed at 20ps, (4) Met408 undergoes a photoreaction from 1 ps to 20 ps, (5) Trp381 is oxidized at 300 ps, with structural changes evolving around it up to 100 μs. B. The kinetics of the observed DED at key positions are shown. For water features the electron density is averaged over positive DED $> 2\sigma$ and for the amino acids over the negative DED $< 2\sigma$ (side chains only). The radius of intergration was 2.5 Å. Wat1 corresponds to feat IV, wat2 to feat V. The kinetics for water and Asn403 are vertically offset.

in time. The temporal response is more complex than expected, with the response of Asp397 decaying faster than the expected lifetime of the FAD^- and the structural response of the waters and Asn403 on the opposing side of the chromophore (Fig. 4B). The side chain movements are somewhat faster than that of the waters, which is complex in itself (see above). Once the new water network is established around the FAD, the side chain of Asp297 can relax. This is reminescent of the compensatory movements of the corresponding residues in a CPD photolyase, which were observed on microsecond

time scales by time-resolved SFX [34].

Further down the charge transport chain, Met408 is of special interest (event 4, Fig. 4A). Met408 is conserved among animal photolyases and in the wider family it may be replaced by a glutamine (Fig. Extended Fig. 3). The photoreaction of Met408 is timed from 1 ps to 20 ps by our measurement. One possibility is that Met408 participates directly in the electron transfer chain as an transient electron donor, or that its oxidation is a by-product of the transient charge that resides on the nearby Trp384. In any case, it is required that a charge has been transferred to this second tryptophan within 1 ps, which is faster than expected. The transfer times from the second to the first tryptophan has been determined to 80 ps in *E.coli* CPD and 9 ps, or less than 35 ps in (6-4) photolyases [12, 37, 42]. We note that the spectroscopic determination of electron transfer times is not straight forward, since the signals from the tryptophans are almost identical. Fast transfer time of less than 1 ps can be explained by coherent tunneling through the first two tryptophans of the tetrad [20] and would be consistent with the spectroscopic data if coherent delocalization is considered. To the best of our knowledge, Met408 has not been proposed to be an active element in the photolyase charge transfer chain, but has recently been implicated in stabilization of charged FAD in a LOV domain protein [43]. We suggest that the response facilitates long-ranged charge separation. Methionines seem ideal for this, because they can be reversibly oxidized and thus fulfill the requirement of photolyases to separate charges without trapping them [44].

At the end of the electron transfer chain the final tryptophan Trp381 shows a surprisingly fast signal, starting from 20 ps (Fig. 4B). This may be consistent with spectroscopic results for the *X.laevis*(6-4)photolyase, which suggested that the fourth electron transfer take place within ≈40 ps [42]. At 20 ps and 300 ps the signal appears directly on the Trp side chain and at 100 μs it has spread to nearby residues, demonstrating a larger structural response than the other sites (event 5, Fig. 4A), similar to what has been observed for a CBD photolyase and by us for the present (6-4) photolyase at 100 ms [34, 35]. Apparently, the protein sequence and structure around Trp381 provide plasticity and movements can occur; while at the other sites, the protein scaffold is much more rigid. This illustrates how evolution has optimized the protein sequence around the charge transfer sites as to achieve efficient charge separation.

At this time, the structural photoresponse of photolyases have been characterized on on nano- to microseconds [34] and milliseconds after photoexcitation [35]. The present work adds the femtosecond to picosecond response to this. Because of the different delay times, all three studies complement each others. A common focal point of response is Asn403 and the salt bridge Asp397:Arg368. Here we establish that the two sites react in coordinated ways around the FAD on picosecond time scales, which is reminescent of the their response on microseconds[34]. The structural response of the tryptophans itself is mute (this work), and but significant changes are observed around the final tryptophan (this work and [34]).

4 Conclusion

We report the ultrafast structural changes that occur in an eukaryotic (6-4) photolyase after photoreduction of FAD to $FAD^{\cdot -}$. Crystallographic snapshots on femto- to picosecond time scales reveal distinct protein conformational rearrangements close to the active sites involved in charge transfer. Side chains and water movements act in concert to stabilize the photoinduced electron on FAD and to drive charge separation. These features have evolved to stabilize the radical pairs as to provide for efficient charge generation and to avoid recombination, but not to trap the charges too deeply in one of the sites. Most conformational changes of the protein environment are driven by changes in electrostatics. We show that the events are timed with respect to each other, which suggests that the proteins have not only evolved for optimal positioning, flexibility, and electrostatics of the charge transfer sites, but also that optimal picosecond dynamics have been selected. The structural dynamics provide a showcase for the active and highly specific involvement of the protein matrix in charge transfer reactions, which we envisage to be not only important for for DNA repair, but also for the many other enzymatic processes that rely on charge transfer.

5 Material and Methods

5.1 Protein expression and crystallization

A pET21d+ plasmid containing a codon optimized gene for *D.m*(6-4)photolyase was used and transformed in BL21(DE3) *E.coli* strain for expression. The cells were grown in a Studier-like medium (supplemented with 50 μg/mL carbenicillin) for few hour at 37°C and moved to 20°C for overnight expression. Cells were lysated through sonication, the supernatant was collected after 30-40 min centrifugation at 35.000 rpm and loaded on a Heparin column (cytiva). The selected elution fractions were then loaded on a Superdex 16/600 column for further purification steps. For detailed information about the purification steps, we refer to the paper [35]. The protein was tested for photoactivity with a 445 nm LED and the reactive fractions of the proteins were employed for crystallization. For the microcrystal preparation, macrocrystals were produced through vapour-diffusion technique in hanging drop plates. Few crystals were grown in 2 days and used to seed the remaining drops by means of a cat-whisker. New crystals were grown within a couple of hours from the striking. The macrocrystals were then crushed and used for batch crystallyzation. We refer to paper [35] for more details on microcrystallization of *D.m*(6-4)photolyase.

5.2 Data aquisition

Data were collected at the Alvra instrument at the SwissFEL. X-ray pulses with a photon energy of 12.06 keV and a pulse energy of 455 to 510 μJ at a repetition rate of 100 Hz were used for the experiment. The microcrystals were dispersed in 22% hydroxyethyl cellulose (HEC) which was extruded at 5μm/min from a capillary with 75 μm inner diameter. For optical excitation a laser pulse of 150 fs duration at

a center wavelength of (474±12.5) nm, with a total energy of 9.6 μJ in a focal spot of 80 × 86.4 μm^2 ($1/e^2$) beam was used. The laser fluence was 1.4 mJ/mm^2. A dark dataset was collected and afterwards data sets with a delays of 400fs, 1ps, 2ps, 20ps, 300ps and 100 μs in respect to a 474 nm laser were recorded. We recorded 42547 indexable frames for the dark, 21576 for the 400 fs time delay, 55898 for 1 ps, 52708 for 2 ps, 98625 for 20 ps, 31979 for 300 ps and 31505 for 100 μs.

5.3 Data processing and analysis

Peak finding and indexing was performed with CrystFEL with the command "–indexing=xgandalf –peaks=peakfinder8 –threshold=4000 - –int-radius=2,3,6 –min-snr=3.5 –min-peaks=8 –min-pix-count=2 –min-res=800 –tolerance=10,10,10,8 –median-filter=3" [45]. The stream file was then used as input to Ambigator with "-y 4/m -w 4/mmm –highres=1.7 –lowres=10 –iterations=10". Later, the ambigator output was fed to Partialator for scaling and postrefinement processes. We used xsphere as model for treating partialities. The hkl rfelections file was then converted to a mtz file and the mtz from each time point was used for calculation of the difference electron density maps (DED maps).

The DED maps are the real-space representation of the difference structure factor amplitudes $|\Delta Fo(light-dark)| = w(|Fo(light)|-|Fo(dark)|)$ and phases from the dark model [31]. The weighting factor (w) was determined for each reflection to reduce the effect of outliers with respect to each reflection[46]. DED maps were calculated with 16 Å and 1.9 Å as a low- and high resolution cutt-off, respectively.

The structure factor in the dark was initially used to obtain a structure of the protein in the resting state. We employed PHENIX for the structure refinement[47]. Before each run of refinement, manual adjustments were carried out in coot [48]. We used the model 3CVY for molecular replacement in PHENIX.

To generate structural models of the photoinduced structural changes, we used real-space refinement in COOT [48] against maps computed from $2F_e$-F_c. F_e is the extrapolated structure factor and was estimated as $F_e = F_c^{dark} + 1/r\Delta F_o$, where F_c^{dark} denotes the calculated structure factor from the model refined against F_o^{dark} [30]. If the photoactivation level (r) is known, F_e represents the structure of the pure photoexcited species. In order to emulate the appropriate activation factor for real space refinement in coot, one should use $r/2$ when computing the F_e, since the refinement in coot is against $2F_e - Fc$, which reduced the effect of photoactivation on the map by approximately 50 %.

In order to estimate the activation factor in the data, we computed extrapolated maps at different r. The mean electron density for all features below -2σ of the extrapolated maps $FT(F_e)$ were plotted against r (Extended Fig. 5) [49]. Linear fits were applied to the linear (solid lines) and extrapolated regions (dashed lines). The point at which the two fitted lines intersect estimates the percentage of protein that is activated. The activation factor was for all time points was 14% (see Extended Fig. 5). We employed an extrapolated map computed at r = 7%, since we used maps from $2F_e - Fc$ for the real space refinement in COOT [48].

After refinement, the accuracy of the structural models was evaluated by comparison between

Table 2: Data and refinement statistics.

	dark	400fs	1ps	2ps	20ps	300ps	100us
PDB code	8C1U	8C6F	8C6A	8C6H	8C6B	8C6C	8C69
Space group	P 41			P 41			
Cell constants							
a, b, c (Å)	103.90 103.90 52.19			103.90 103.90 52.19			
α, β, γ (°)	90.0 90.0 90.0			90.0 90.0 90.0			
Resolution (Å)†	16.93 – 1.70 (1.70-1.71)			15.72-1.9 (1.90-1.91)			
Data completeness (%)†	99.99 (100)	99.99 (99.89)	100.00 (100.00)	100.00 (100.00)	99.99 (100.00)	99.99 (99.94)	99.99 (100)
R_{split} (%) †	12.05 (95.37)	15.50 (51.13)	9.11 (28.99)	9.49 (27.85)	7.28 (21.15)	10.68 (35.90)	11.85 (41.41)
CC* †	0.99 (0.77)	0.99 (0.88)	0.99 (0.95)	0.99 (0.96)	0.99 (0.97)	0.99 (0.94)	0.99 (0.92)
$< I/\sigma(I) >$ †	6.89 (1.18)	6.53 (2.29)	10.97 (3.55)	10.86 (3.89)	13.90 (5.19)	9.52 (3.02)	8.76 (2.87)
Multiplicity †	352.35	56.25	181.74	165.24	275.96	100.12	88.90
Number of hits	465000	306939	510943	423684	649772	297154	392837
Number of indexed hits	63249	21576	55898	52708	98625	31979	31496
Number of total reflection	21652613	2482657	8021949	7293598	12181270	4419046	3923924
Number of unique reflections	61453 (2414)	44136 (1764)	44138 (1766)	44138 (1766)	44140 (1766)	44136 (1765)	44135 (1766)
Refinement							
R_{work}/R_{free}	0.170-0.197	0.291-0.327	0.251-0.270	0.244-0.274	0.227-0.241	0.247-0.281	0.263-0.300
Wilson B-factor (Å^2)	18.2	3.4	5.6	5.9	7.4	5.1	4.8
Total number of atoms	4350	4300	4298	4298	4299	4297	4300
Average B, all atoms (Å^2)	33.0	20	33	20	20	20	18
R.m.s deviations							
Bond lengths (Å)	0.011	0.007	0.003	0.007	0.007	0.008	0.008
Bond angle (°)	1.170	0.832	0.643	0.894	0.886	0.935	0.871

† Highest resolution shell is shown in parenthesis.

the real-space maps of observed ΔF_o and calculated ΔF_c=F_c^{light} - F_c^{dark} structure factors. We also computed the Pearson correlation coefficient (CC) in real space as $CC = cov(map1, map2)/(\sigma_{map1} * \sigma_{map2})$, where σ denotes the standard deviation of the map. Increasing CC values indicate better agreement.

6 Author contributions

SW conceptualized the study; SW, AC and WYW designed the experiments; AC and WYW prepared the protein crystals, all authors performed the experiment at the SwissFEL Alvra beamline; AC, WYW, MKS, AN, SW, TW, and MS analyzed the data; AC and SW wrote the paper with input from all authors.

7 Data availability statement

The SFX data generated are available through the CXIDB database. The structural models will be made available through the Protein Data Bank (currently submitted and accepted, but not released).

8 Extended Data

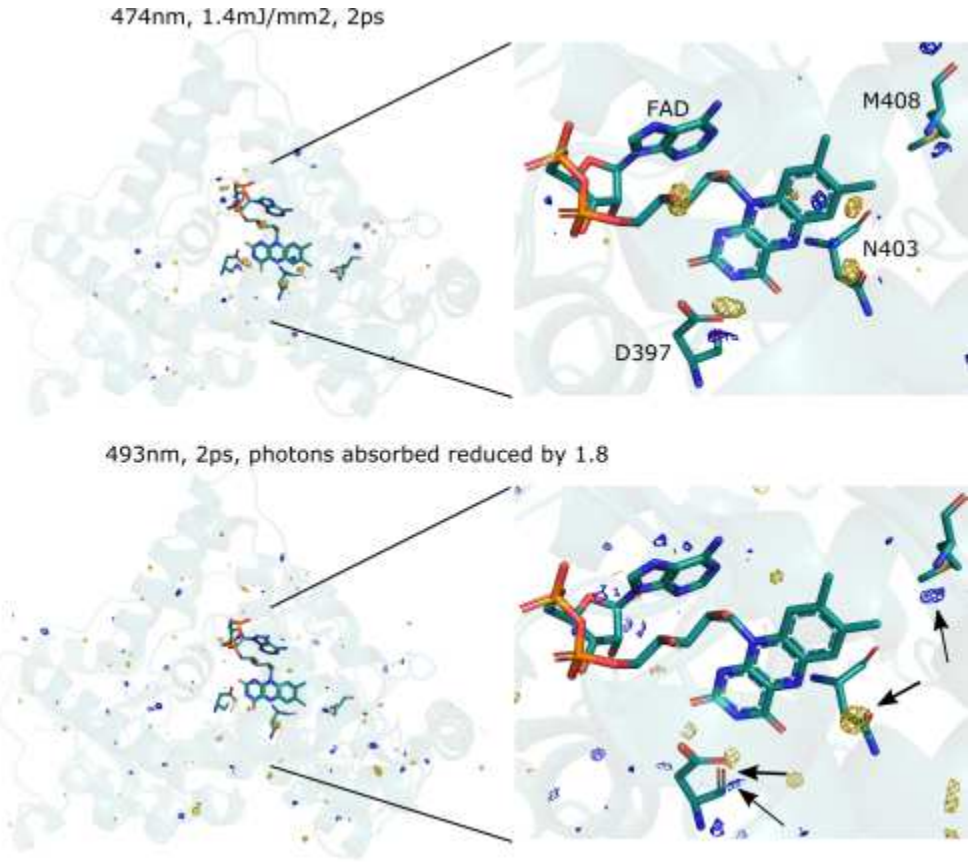

Extended Figure 1: Lowering the photon flux by a factor 1.8 reduced the DED signal. The upper panels show the DED presented in the main paper at 2 ps (photoexciation at 474 nm, 1.4 mJ/mm^2). The lower panels show a DED map recorded at 2 ps after photoexcitation at 493 nm (2.9 mJ/mm^2). The maps are contoured at 0.012 eÅ^{-3} (upper) and 0.014 eÅ^{-3} (lower) respectively. Because 493 nm is at the red onset of absorption and a the overlap between the spectrum of the laser pulse and the absoprtion is poor, the number of absorbed photons is expected to be lower at 493 nm. We estimate that the overlap integral between laser and the absorption of the photolyase was 3 times lower at 493 nm compared to excitation at 474 nm (assuming a Gaussian spectrum of the laser). Thus, the number of absorbed photons is expected to be 1.8 times lower (2.9/3 mJ/mm^2 in the map at 493 nm compared to 1.4 mJ/mm^2) for the map at 474 nm), which explains why it has a lower DED signal amplitude. In a third measurement at even lower excitation fluence (1.1/3 mJ/mm^2 at 493 nm), we did not find any DED signals above noise. We note that the extinction coefficient of the FAD is low (approx. 10000 $M^{-1}cm^{-1}$ at λ_{max}) compared to for example rhodopins approx. 60000 $M^{-1}cm^{-1}$), where similar or higher excitation fluences were used in SFX experiments [30]. Thus, we conclude that the excitation fluence of 1.4 mJ/mm^2 at 474 nm used for all measurements in the main paper was within the one photon regime.

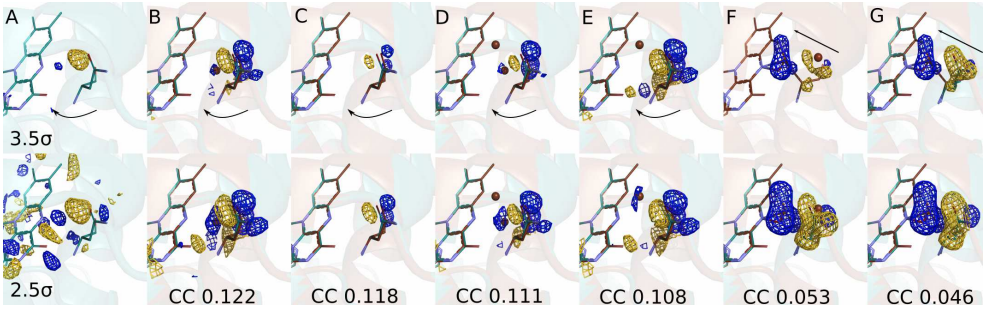

Extended Figure 2: Alternative models for the 300 ps structure do not lead to good agreement between observed (A) and calculated (B-G) difference electron density at 300ps. Each map is shown at two different sigma levels (upper and lower row). We modelled and computed calculated difference map of Asn403 with two water molecules (D), one water molecule at different positions (B and E) and without water molecule (C). The Pearson Correlation Coefficient (CC) values change only moderately between models B-E and we therefore present the simplest model (without water, C) in the main paper. Alternative to the models with water, we moved the Asn403 closer to the FAD (G) and placed a water nearby (F). The experimental DED is not reproduced and the CC drops drastically for models E and F. The Pearson Correlation Coefficient (CC) values calculated between the observed and calculated DED within a sphere of 7 Å radius centred on Asn403 are shown. Gold indicates negative and blue positive DED.

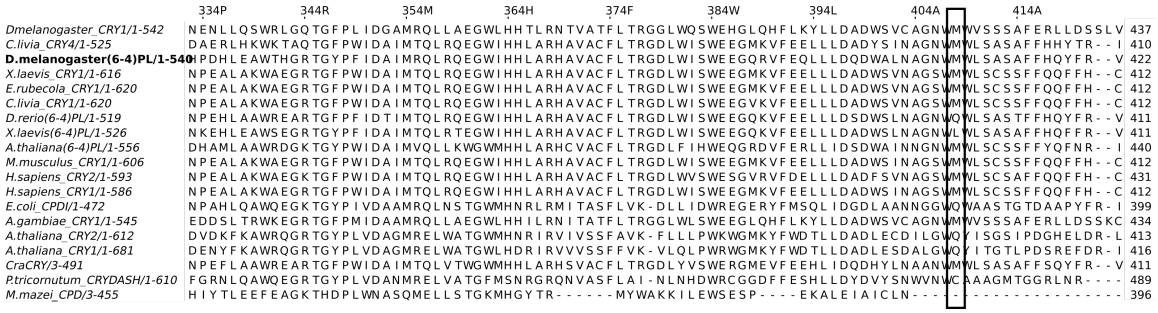

Extended Figure 3: Sequence alignments of some members of (6-4)photolyase, animal and plant cryptochromes and bifunctional CRY-DASH. The sequence alignment reveals that Met408 is conserved among animal cryptochromes.The alignment was performed in Jalview 2.11.1.4 with Clustal using the default settings.

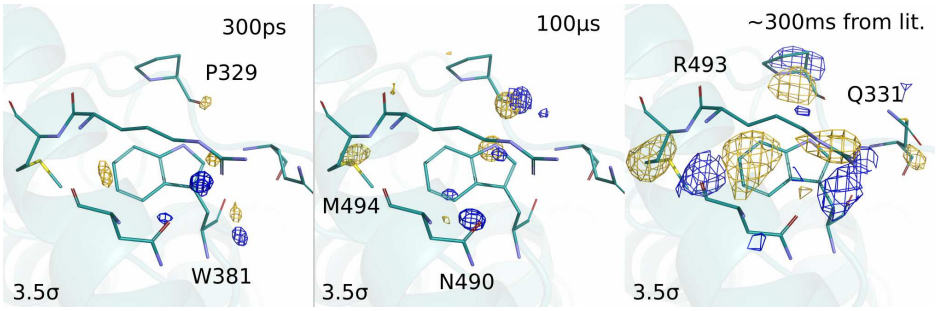

Extended Figure 4: Observed difference electron density maps at 300 ps and 100 μs around the last tryptophan (Trp381). The electron densities were compared to previously published data [35].

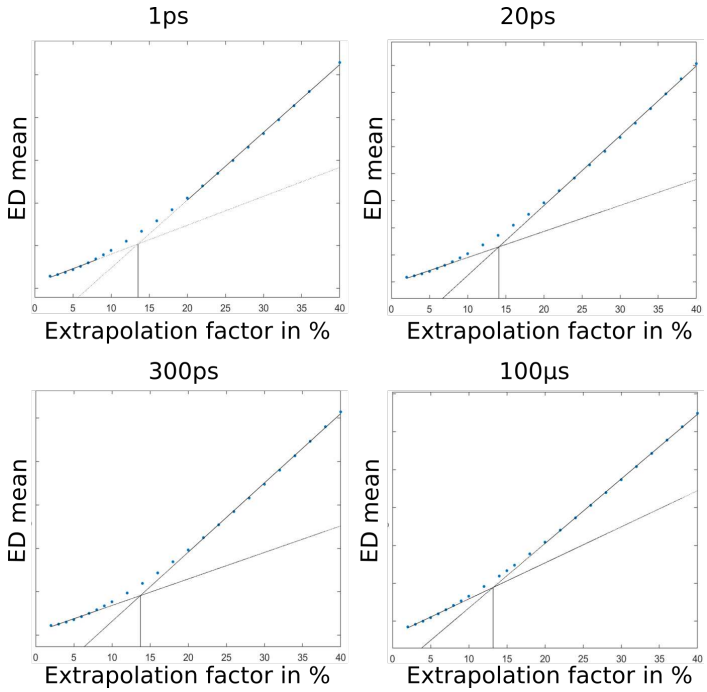

Extended Figure 5: Negative features plotted as function of the percentage of activation (r) for the 1 ps, 20 ps, 300 ps and 100 μs maps. The point of intersection in the extrapolated (dashed lines) linear fits (solid line) determines the level of activation.

References

1. Babcock, G. T. & Wikström, M. Oxygen activation and the conservation of energy in cell respiration. *Nature* **356,** 301–309. ISSN: 1476-4687. https://www.nature.com/articles/356301a0 (6367 1992).

2. Dawson, J. H. Probing Structure-Function Relations in Heme-Containing Oxygenases and Peroxidases. *Science* **240,** 433–439. ISSN: 00368075. https://www.science.org/doi/10.1126/science.3358128 (4851 1988).

3. Hochstein, L. I. & Tomlinson, G. A. The enzymes associated with denitrification. *Annual Reviews in Microbiology* **42,** 231–261 (1988).

4. Gray, H. B. & Winkler, J. R. ELECTRON TRANSFER IN PROTEINS. *Annual Review of Plant Biology* **65,** 537–561. ISSN: 00664154. https://www.annualreviews.org/doi/abs/10.1146/annurev.bi.65.070196.002541 (Nov. 2003).

5. Barbara, P. F., Walker, G. C. & Smith, T. P. Vibrational modes and the dynamic solvent effect in electron and proton transfer. *Science* **256,** 975–981. ISSN: 00368075 (5059 1992).

6. Sancar, A. Structure and function of DNA photolyase and cryptochrome blue-light photoreceptors. *Chemical reviews* **103,** 2203–2238 (2003).

7. Vaidya, A. T. *et al.* Flavin reduction activates Drosophila cryptochrome. *Proceedings of the National Academy of Sciences of the United States of America* **110,** 20455–20460. ISSN: 00278424. https://www.pnas.org/doi/abs/10.1073/pnas.1313336110 (51 Dec. 2013).

8. Aubert, C., Vos, M. H., Mathis, P., Eker, A. P. & Brettel, K. Intraprotein radical transfer during photoactivation of DNA photolyase. *Nature* **405,** 586–590 (2000).

9. Rupert, C. S., Goodal, S. H. & Herriott, R. M. PHOTOREACTIVATION IN VITRO OF ULTRAVIOLET INACTIVATED HEMOPHILUS INFLUENZAE TRANSFORMING FACTOR. *The Journal of General Physiology* **41,** 451. ISSN: 00221295. /pmc/articles/PMC2194849/?report=abstract%20https://www.ncbi.nlm.nih.gov/pmc/articles/PMC2194849/ (3 Jan. 1958).

10. Chaves, I. *et al.* The Cryptochromes: Blue Light Photoreceptors in Plants and Animals. *Annual Review of Plant Biology* **62,** 335–364. ISSN: 15435008. https://www.annualreviews.org/doi/abs/10.1146/annurev-arplant-042110-103759 (Apr. 2011).

11. Mouritsen, H. Long-distance navigation and magnetoreception in migratory animals. *Nature* **558,** 50–59. ISSN: 1476-4687. https://pubmed.ncbi.nlm.nih.gov/29875486/ (7708 June 2018).

12. Liu, Z. *et al.* Determining complete electron flow in the cofactor photoreduction of oxidized photolyase. *Proceedings of the National Academy of Sciences* **110,** 12966–12971 (2013).

13. Liu, Z., Wang, L. & Zhong, D. Dynamics and mechanisms of DNA repair by photolyase. *Physical Chemistry Chemical Physics* **17,** 11933–11949 (2015).

14. Weber, S. Light-driven enzymatic catalysis of DNA repair: a review of recent biophysical studies on photolyase. *Biochimica et Biophysica Acta (BBA)-Bioenergetics* **1707,** 1–23 (2005).

15. Müller, P., Ignatz, E., Kiontke, S., Brettel, K. & Essen, L.-O. Sub-nanosecond tryptophan radical deprotonation mediated by a protein-bound water cluster in class II DNA photolyases. *Chemical science* **9,** 1200–1212 (2018).

16. Zhang, M., Wang, L. & Zhong, D. Photolyase: Dynamics and electron-transfer mechanisms of DNA repair. *Archives of Biochemistry and Biophysics* **632,** 158–174. ISSN: 0003-9861 (Oct. 2017).

17. Marcus, R. A. Electron Transfer Reactions in Chemistry: Theory and Experiment (Nobel Lecture). *Angewandte Chemie International Edition in English* **32,** 1111–1121. ISSN: 1521-3773. https://onlinelibrary.wiley.com/doi/full/10.1002/anie.199311113%20https://onlinelibrary.wiley.com/doi/abs/10.1002/anie.199311113%20https://onlinelibrary.wiley.com/doi/10.1002/anie.199311113 (8 Aug. 1993).

18. Sumi, H. & Marcus, R. A. Dynamical effects in electron transfer reactions. *The Journal of Chemical Physics* **84,** 4894. ISSN: 0021-9606. https://aip.scitation.org/doi/abs/10.1063/1.449978 (9 June 1998).

19. Rafiq, S., Fu, B., Kudisch, B. & Scholes, G. D. Interplay of vibrational wavepackets during an ultrafast electron transfer reaction. *Nature chemistry* **13,** 70–76. ISSN: 1755-4349. https://pubmed.ncbi.nlm.nih.gov/33288893/ (1 Jan. 2021).

20. Cailliez, F., Müller, P., Firmino, T., Pernot, P. & de la Lande, A. Energetics of photoinduced charge migration within the tryptophan tetrad of an animal (6–4) photolyase. *Journal of the American Chemical Society* **138,** 1904–1915 (2016).

21. Woiczikowski, P. B., Steinbrecher, T., Kubař, T. & Elstner, M. Nonadiabatic QM/MM simulations of fast charge transfer in Escherichia coli DNA photolyase. *Journal of Physical Chemistry B* **115,** 9846–9863. ISSN: 15205207. https://pubs.acs.org/doi/abs/10.1021/jp204696t (32 Aug. 2011).

22. Lu, Y., Kundu, M. & Zhong, D. Effects of nonequilibrium fluctuations on ultrafast short-range electron transfer dynamics. *Nature Communications* **11,** 1–9. ISSN: 2041-1723. https://www.nature.com/articles/s41467-020-15535-y (1 June 2020).

23. Zhang, Y., Liu, C., Balaeff, A., Skourtis, S. S. & Beratan, D. N. Biological charge transfer via flickering resonance. *Proceedings of the National Academy of Sciences of the United States of America* **111,** 10049–10054. ISSN: 10916490. /pmc/articles/PMC4104919/%20/pmc/articles/PMC4104919/?report=abstract%20https://www.ncbi.nlm.nih.gov/pmc/articles/PMC4104919/ (28 July 2014).

24. Pal, S. K., Peon, J. & Zewail, A. H. Biological water at the protein surface: Dynamical solvation probed directly with femtosecond resolution. *Proceedings of the National Academy of Sciences of the United States of America* **99,** 1763–1768. ISSN: 00278424. https://www.pnas.org/doi/abs/10.1073/pnas.042697899 (4 Feb. 2002).

25. Chang, C. W. *et al.* Mapping solvation dynamics at the function site of flavodoxin in three redox states. *Journal of the American Chemical Society* **132,** 12741–12747. ISSN: 00027863. https://pubs.acs.org/doi/abs/10.1021/ja1050154 (36 Sept. 2010).

26. Pande, K. *et al.* Femtosecond structural dynamics drives the trans/cis isomerization in photoactive yellow protein. *Science* **352,** 725–729. ISSN: 10959203. http://www.sciencemag.org/cgi/doi/10.1126/science.aad5081 (6286 May 2016).

27. Barends, T. R. *et al.* Direct observation of ultrafast collective motions in CO myoglobin upon ligand dissociation. *Science* **350,** 445–450 (2015).

28. Brändén, G. & Neutze, R. Advances and challenges in time-resolved macromolecular crystallography. *Science* **373.** ISSN: 1095-9203. https://pubmed.ncbi.nlm.nih.gov/34446579/ (6558 Aug. 2021).

29. Hosaka, T. *et al.* Conformational alterations in unidirectional ion transport of a light-driven chloride pump revealed using X-ray free electron lasers. *Proceedings of the National Academy of Sciences* **119,** e2117433119 (2022).

30. Nogly, P. *et al.* Retinal isomerization in bacteriorhodopsin captured by a femtosecond x-ray laser. *Science* **361,** eaat0094 (2018).

31. Claesson, E. *et al.* The primary structural photoresponse of phytochrome proteins captured by a femtosecond X-ray laser. *Elife* **9,** e53514 (2020).

32. Dods, R. *et al.* Ultrafast structural changes within a photosynthetic reaction centre. *Nature* **589,** 310–314 (2021).

33. Mous, S. *et al.* Dynamics and mechanism of a light-driven chloride pump. *Science (New York, N.Y.)* **375,** 845–851. ISSN: 1095-9203. https://pubmed.ncbi.nlm.nih.gov/35113649/ (6583 Feb. 2022).

34. Maestre-Reyna, M. *et al.* Serial crystallography captures dynamic control of sequential electron and proton transfer events in a flavoenzyme. *Nature Chemistry,* 1–9 (2022).

35. Cellini, A. *et al.* Structural basis of the radical pair state in photolyases and cryptochromes. *Chemical Communications* **58,** 4889–4892 (2022).

36. Immeln, D., Weigel, A., Kottke, T. & Perez Lustres, J. L. Primary events in the blue light sensor plant cryptochrome: intraprotein electron and proton transfer revealed by femtosecond spectroscopy. *Journal of the American Chemical Society* **134,** 12536–12546 (2012).

37. Brazard, J. *et al.* Spectro- Temporal Characterization of the Photoactivation Mechanism of Two New Oxidized Cryptochrome/Photolyase Photoreceptors. *Journal of the American Chemical Society* **132,** 4935–4945 (2010).

38. Wickstrand, C. *et al.* A tool for visualizing protein motions in time-resolved crystallography. *Structural Dynamics* **7,** 024701 (2020).

39. Krapf, S., Koslowski, T. & Steinbrecher, T. The thermodynamics of charge transfer in DNA photolyase: using thermodynamic integration calculations to analyse the kinetics of electron transfer reactions. *Physical Chemistry Chemical Physics* **12,** 9516–9525. ISSN: 1463-9084. https://pubs.rsc.org/en/content/articlehtml/2010/cp/c000876a%20https://pubs.rsc.org/en/content/articlelanding/2010/cp/c000876a (32 Aug. 2010).

40. Wijaya, I. M. M., Domratcheva, T., Iwata, T., Getzoff, E. D. & Kandori, H. Single hydrogen bond donation from flavin N5 to proximal asparagine ensures FAD reduction in DNA photolyase. *Journal of the American Chemical Society* **138,** 4368–4376 (2016).

41. Qiu, W. *et al.* Protein surface hydration mapped by site-specific mutations. *Proceedings of the National Academy of Sciences of the United States of America* **103,** 13979–13984. ISSN: 00278424. https://www.pnas.org/doi/abs/10.1073/pnas.0606235103 (38 Sept. 2006).

42. Martin, R. *et al.* Ultrafast flavin photoreduction in an oxidized animal (6-4) photolyase through an unconventional tryptophan tetrad. *Physical Chemistry Chemical Physics* **19,** 24493–24504 (2017).

43. Yee, E. F. *et al.* Peripheral Methionine Residues Impact Flavin Photoreduction and Protonation in an Engineered LOV Domain Light Sensor. *Biochemistry* **60,** 1148–1164. ISSN: 1520-4995. https://pubmed.ncbi.nlm.nih.gov/33787242/ (15 Apr. 2021).

44. Kim, G., Weiss, S. J. & Levine, R. L. Methionine Oxidation and Reduction in Proteins. *Biochimica et biophysica acta* **1840,** 901–905. ISSN: 03044165. /pmc/articles/PMC3766491/%20/pmc/articles/PMC3766491/?report=abstract%20https://www.ncbi.nlm.nih.gov/pmc/articles/PMC3766491/ (2 Feb. 2014).

45. White, T. A. *et al.* CrystFEL: a software suite for snapshot serial crystallography. *Journal of applied crystallography* **45,** 335–341 (2012).

46. Ren, Z. *et al.* A molecular movie at 1.8 Å resolution displays the photocycle of photoactive yellow protein, a eubacterial blue-light receptor, from nanoseconds to seconds. *Biochemistry* **40,** 13788–13801. ISSN: 00062960. https://pubs.acs.org/doi/10.1021/bi0107142 (46 2001).

47. Liebschner, D., Afonine, P. V., *et al.* Macromolecular structure determination using X-rays, neutrons and electrons: Recent developments in Phenix. *Acta Crystallographica Section D Structural Biology* **75,** 861–877 (2019).

48. Emsley, P. & Cowtan, K. Coot: model-building tools for molecular graphics. *Acta crystallographica section D: biological crystallography* **60,** 2126–2132 (2004).

49. Pandey, S. *et al.* Time-resolved serial femtosecond crystallography at the European XFEL. *Nature methods* **17,** 73–78 (2020).

Supplementary Files

This is a list of supplementary files associated with this preprint. Click to download.

- 1ps.txt
- 400fs.txt
- 2ps.txt
- 100us.txt
- 1ps.pdf
- 300ps.txt
- 100microsecond.pdf
- 20ps.pdf
- dark.txt
- 20ps.txt
- 2ps.pdf
- 300ps.pdf
- 400fs.pdf
- dark.pdf